Original Paper

Early View publication on
www.interscience.wiley.com
(issue and page numbers not yet assigned;
citable using Digital Object Identifier – **DOI**)

phys. stat. sol. (b), 1–12 (2006) / **DOI** 10.1002/pssb.200672542

Raman spectroscopy under pressure in semiconductor nanoparticles

B. A. Weinstein*

Department of Physics, SUNY at Buffalo, Buffalo, NY 14260-1500, USA

Received 25 July 2006, accepted 8 August 2006
Published online 30 Novembeer 2006

PACS 62.50.+p, 63.22.+m, 78.30.Fs, 78.67.Bf

A brief survey of recent high-pressure Raman investigations and associated studies of nanoparticle systems is given, and the consequences for understanding the vibrational properties and stability of these systems are reviewed. The results of new pressure-Raman experiments on colloidal ZnSe nanorods, high-purity bulk $^{68}Zn^{76}Se$ crystals, and colloidal InP/CdS core/shell nanoparticles are presented. The nanorod and bulk ZnSe spectra are compared for similar pressure cycles. Evidence is found for the early stages of nucleation of the zincblende-rocksalt transition in the bulk crystals, and for the effects of non-uniform surface contact forces in the nanorod ensemble. Similarities and differences between the post-transition spectra of both types of samples are discussed. The InP/CdS core/shell nanoparticles exhibit a structured Raman line-shape that contains contributions from LO- and TO-like modes of the InP cores and from an overlapping manifold of CdS shell modes. Our results indicate that pressure acts to decrease this overlap. Cross-interface mechanical coupling is considered for describing the pressure-induced line-shape changes.

1 Introduction

Nanocrystalline semiconductor systems offer fascinating opportunities to explore basic phenomena related to phonon and electron confinement [1, 2], electron–phonon interactions and polaron effects [3, 4], phonon mixing and decay under confined conditions [5, 6], magnetic interactions [7], volume and surface disorder [8], and structural stability [9]. Equally intriguing are the possibilities to utilize these phenomena in a host of novel applications ranging from traditional LED photonics [10] to biological flourescence markers [11] and spin coupled quantum devices [7]. In the former two cases, development has advanced to practical stages.

With regard to high-pressure investigations of nanoparticle systems, a wide range of semiconductor materials belonging to Groups IV, III–V, II–VI, and oxides have been investigated [12–19], including nanoparticles in colloidal solution and glass matrices, epitaxially grown quantum-dots, porous semiconductors, and nano-domains created by indentation, pulverization, or high-pressure phase transitions in bulk crystals [20–25]. In those studies, Raman spectroscopy (combined with other X-ray and optical methods) has played a significant role – in detecting the onset of pressure-induced transitions, identifying confined and surface modes, measuring the Gruneisen parameters of those modes, and assessing the size of nanoparticles domains. We shall focus (due to length constraints) on several illustrative examples.

* e-mail: phyberni@buffalo.edu, Phone: +01 716 645 2017, Fax: +01 716 645 2507

1.1 Early work

A number of the important early studies were directed at questions related to phase stability. Pressure Raman experiments carried out on CdSe [26], CdS [27], and CdS_xSe_{1-x} [16] nanoparticles, either in solution or in glass matrices, were instrumental in establishing that the high pressure transition threshold P_T was elevated in smaller nanocrystals. The Raman signatures of the low-pressure phase were observed to well above the bulk P_T, e.g., to 6.5 and 8 GPa in 4 nm diameter zincblende CdS particles capped with different surfactants (polyphosphate and tetrabutylammonium-EDTA, respectively) compared to $P_T \sim 2.7$ GPa in bulk CdS. The variation of P_T for different capping agents indicates the importance of surface properties for nanoparticle stability. The transition threshold to the high pressure structure (for the same surfactant) was systematically higher in smaller nanocrystals. The systematic size-dependence of P_T for CdSe nanoparticles at 300 K (using the hysteresis midpoint from optical density vs. pressure curves) is shown in Fig. 1 [28].

In these studies, the rates of pressure shift of the Raman frequencies in hydrostatic (or quasi-hydrostatic) media tended to be close to the corresponding bulk values, and generally did not show a strong size variation. This was interpreted as indicating that the effective interatomic (and elastic) potentials within the core of nanocrystals are insensitive to surface constraints [16, 20]. The situation is quite different for self-assembled Ge quantum dots in Si/Ge short period superlattices [13, 29]. Here the pressure shift of the Ge–Ge Raman frequency is found to be ~25% less rapid than for bulk Ge crystals. In this epitaxial system the strain transmitted to the Ge dots under the applied pressure is controlled by the Si matrix, and so is smaller than would be felt in bulk Ge.

Figure 2 displays high-resolution transmission electron micrographs (TEM) of two nearly spherical CdSe nanocrystals (~6 nm diameter) prepared in the same colloidal synthesis. The stabilizing agent (surfactant capping material) was trioctylphosphine oxide. The left and right hand pictures show representative particles at 1 atm, a) prior to pressurization, and b) after cycling through the rocksalt phase transition, respectively [30].

Note that the as-grown nanocrystals are predominantly in the wurtzite phase, but contain stacking faults that correspond to zincblende regions. After the rocksalt transition the nanocrystals revert back to a 4-fold tetrahedral coordination at 1 atm, but there is now a stronger mix of the zincblende component. In this sense the transition is primarily a 4-fold to 6-fold bonding change.

In a series of papers Alivisatos and co-workers (see e.g., [9, 12, 26, 31]) were able to show that the phase transitions in nanocrystals of diameters smaller than ~10–15 nm were usually found to transform as single domains in both the forward and reverse directions.

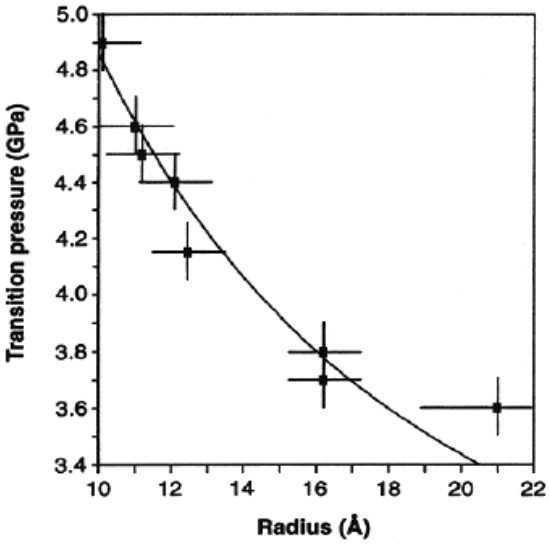

Fig. 1 P_T vs. particle radius for wtz-rs transition in CdSe nanocrystals. Reprinted with permission from Ref. [28]. Copyright 1994 AAAS.

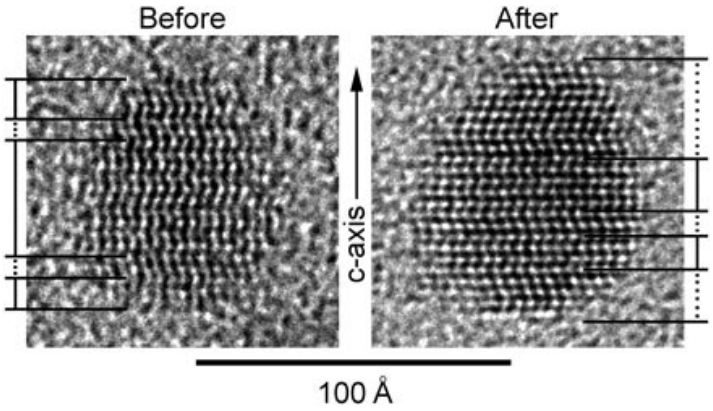

Fig. 2 HR-TEM photos of typical CdSe nanocrystals before and after their phase transitions. Wurtzite (solid lines), zincblende (dotted lines). Reprinted with permission from Ref. [9]. Copyright 2001 AAAS.

They concluded that the elevated phase transition pressure (Fig. 1) of isolated nanoparticles was due to an increase in their surface energy associated with the change to a structure with greater coordination. The extra surface energy arises from higher-indicii crystal facets and shape distortions that develop during the transformation. This affects both the kinetics and the equilibrium boundary of the transitions [12]. Based on simulations of X-ray diffraction lineshapes for CdSe nanoparticles, they proposed a martinsitic type mechanism for the transition from 4-fold (zincblende or wurtzite) to 6-fold rocksalt [31]. The mechanism involves slip motion of alternate (111) planes in anti-parallel directions (Fig. 3). They note that the proposed path, though certainly not unique, explains the data rather well.

These pressure-induced single-domain transformations in nanoparticles differ considerably from the transitions in bulk semiconductors. In the bulk crystals the analogous bonding changes nucleate at multiple cites, and then grow once the pressure becomes high enough for the $P\Delta V$ term ($-\Delta V$ is $\sim 10-20\%$) to overcome kinetic barriers associated with the transition path. Unlike the nanoparticles, these barriers must include surface energy terms of the nuclei surrounded by a matrix of the low-pressure structure. This nucleation process leads to transformed phases that are polycrystalline, a property that has been applied to fabricate nanocrystalline systems by multiple high-pressure cycling of bulk material through the forward and reverse transitions [25, 32]. Clearly grain boundary effects must be considered in order to understand the surface energetics and surface structure of the nanocrystal domains in transformed bulk crystals.

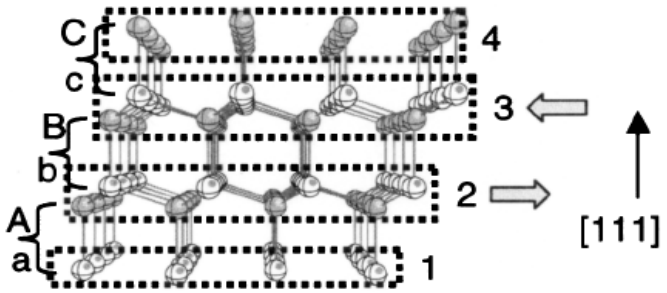

Fig. 3 Proposed 4-fold to 6-fold transition path in CdSe nanocrystals. Alternate (111) planes slide in opposite directions. Reprinted with permission from Ref. [31]. Copyright 2000 APS.

2 Phonons and phase transformations in ZnSe bulk crystals and nanoparticles

2.1 Bulk $^{68}Zn^{76}Se$ crystals

An example of such effects has recently been explored by the author and co-workers in comparative pressure-Raman experiments on isotope pure $^{68}Zn^{76}Se$ bulk crystals and colloidal ZnSe nanorods. The work grew out of prior studies of resonant anharmonic processes in bulk semiconductors [33–35]. We observed that the effects of pressure-on the Raman spectra of $^{68}Zn^{76}Se$ crystals recorded at 11 K and at 300 K exhibited striking differences, quite unlike what was found in earlier work on ZnS [33]. The ZnSe results are summarized in Figs. 4 and 5.

The 11 K spectra (Fig. 4) are well understood. The gradual broadening and lack of structure in the TO(Γ) and LO(Γ) line-shapes as a function of pressure result from the positions of these modes relative to a gap in the two-phonon density of states (DOS). (See e.g., the calculated DOS in Ref. [36].) For ZnSe the TO(Γ) and LO(Γ) lines stay inside this DOS gap, advancing to a more populated region of TA + LA combinations, but not crossing any strong critical-point features. Perturbation theory predicts

$$I(\omega) \propto \frac{\Gamma(\omega)/2}{[\omega - \omega_0 - \Delta(\omega)]^2 + [\Gamma(\omega)/2]^2} \quad \text{with} \quad \Gamma(\omega) = |V_3|\, \rho^{(2)}(\omega)\, [1 + n(\omega_1) + n(\omega_2)]\,, \tag{1}$$

for the form of the TO(Γ) and LO(Γ) line-shapes, where, V_3 is a coupling strength, $\rho^{(2)}(\omega)$ is the 2-phonon DOS, and the n are thermal factors. Hence, the pressure behavior of these profiles in ZnSe reflects the featureless shape of $\rho^{(2)}(\omega)$ inside the DOS gap. This differs from ZnS, where TO(Γ) enters a similar DOS gap only for $P > 9$ GPa, and shows line-shape features due to crossing TA + LA singularities at lower pressures [33].

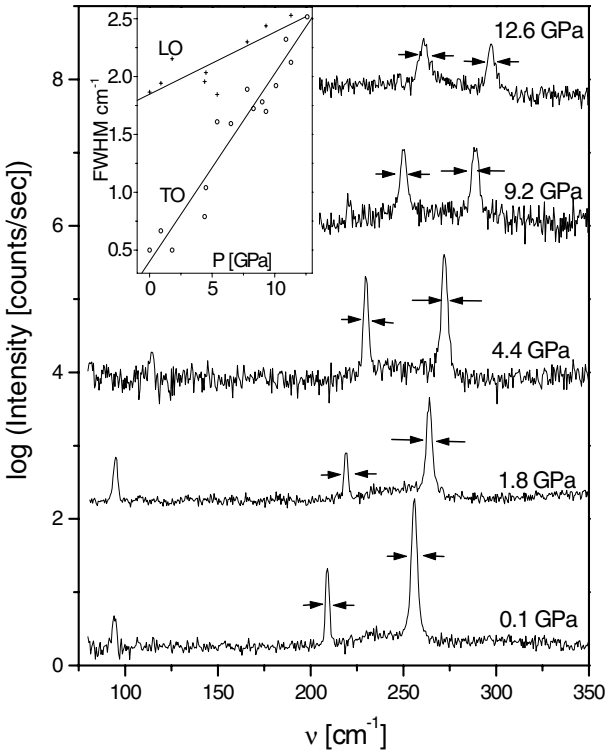

Fig. 4 Effect of pressure on the TO(Γ) and LO(Γ) Raman peaks in a bulk $^{68}Zn^{76}Se$ crystal at 11 K. Note log intensity scale. Arrows mark FWHM plotted in inset.

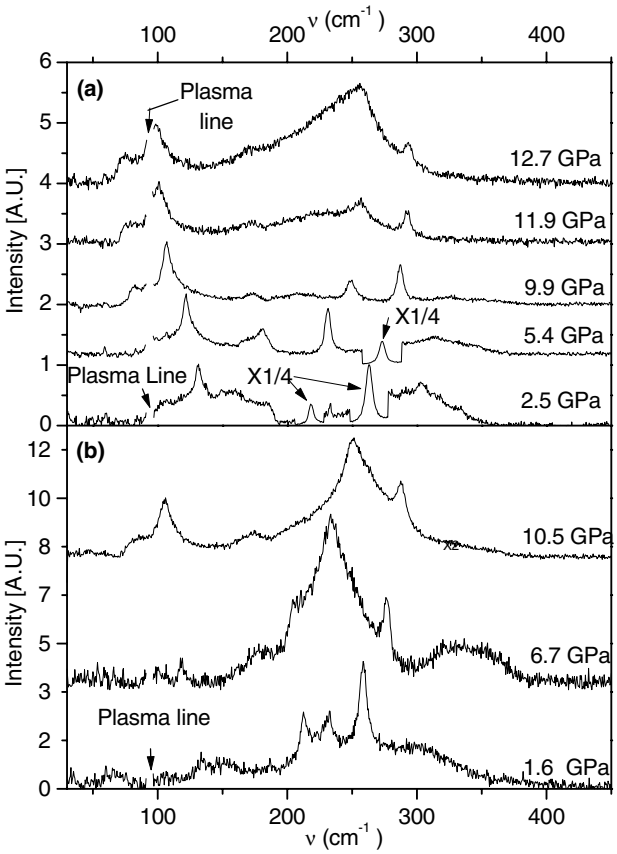

Fig. 5 Raman spectra of bulk $^{68}Zn^{76}Se$ at 300 K for (a) increasing pressure, and (b) decreasing pressure after the phase transition. Nos. 1–4 label LO(Γ), TO(Γ), 2TA(X), 'new peak'. λ_L = 647 nm except for 514 nm at 10.5 GPa.

The 300 K Raman results for $^{68}Zn^{76}Se$ (Fig. 5a) exhibit very strong broadening at pressures above ~11 GPa in a region centered about the TO(Γ) peak [37], while reasonably sharp LO(Γ) and 2TA(X) peaks persist. This broadening under pressure seems too large to be explained by resonant 3-phonon mixing. It is qualitatively different than the behavior in ZnSe at 11 K (Fig. 4), and larger than seen in other materials [33–35]. Rather, we attribute it to disorder and localization in ZnSe associated with the early stages of nucleation of 6-fold coordinated domains, and related grain boundary effects. The continued presence of a sharp but weaker LO(Γ) component is consistent with fragmentation of the ZnSe sample into small domains. These results indicate that the zincblende-rocksalt transition in ZnSe is strongly affected by kinetics factors; perhaps the ability to generate point defects in ZnSe is invovled. Additional pressure-temperature experiments are clearly of interest to explore the activation energies.

On decreasing pressure at 300 K (Fig. 5b) after the phase transition (observed visually at ~13.6 GPa), the main zincblende features return, including the sharp TO(Γ) peak in the 1.6 GPa trace. However, the broadening is still evident at that pressure, and a new sharp peak appears between TO(Γ) and LO(Γ). The new peak indicates retention of a metastable phase in domains of the cycled bulk sample. The cinnabar and wurtzite structures, both close in energy to zincblende and common in pressure-cycled II–VI materials [38, 39], are prime candidates. The new peak is also close to (within 7 cm^{-1}) the right frequency to be assigned to Se precipitates [40].

2.2 ZnSe nanorods

A number of experimental and theoretical results suggest that bulk semiconductors cycled through their high-pressure transitions can acquire the localization properties of disordered nanocrystalline systems [8,

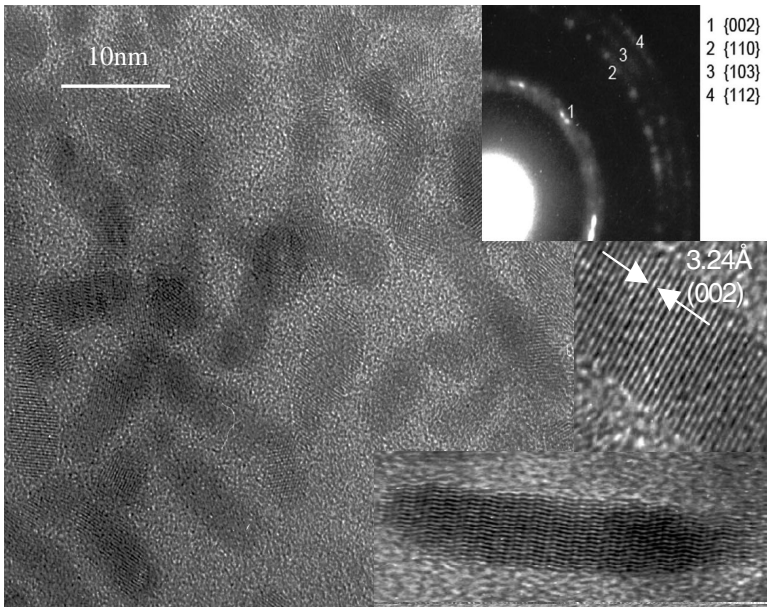

Fig. 6 TEM and ED photos of ZnSe nanorods studied here. Wurtzite structure is dominant but stacking faults indicate some zincblende.

24, 25, 32, 41]. To further explore the relationship between the phonon properties of bulk and nanoparticle ZnSe as a function of pressure and pressure-cycling, Raman experiments were carried out on a ZnSe nanorod ensemble prepared by colloidal chemistry using oleic acid as the surfactant. The sample was precipitated as a powder and kept under vacuum until loading in the diamond-anvil cell with a 4:1 methanol:ethanol pressure medium. From TEM and electron diffraction studies (Fig. 6), the sample ensemble contained ~5 nm × 15–25 nm nanorods, many having mixed wurtzite-zincblende structure, and some agglomerated clusters. Figure 7 summarizes the pressure-Raman results.

In Fig. 7a the low pressure spectra are typical of II–VI nanorods [42], showing LO-like and TO-like peaks, shifted by confinement slightly down and up from the bulk frequencies, respectively. Two peaks are observed distinctly up to 3.5 GPa. Their pressure-shifts are ~4 cm^{-1}/GPa for the LO-like peak and ~5 cm^{-1}/GPa for the TO-like peak (accurate to ±20%), similar to the bulk pressure coefficients. Above 3.5 GPa the spectrum broadens into a single peak. The up-stroke phase transition was observed by visual darkening at 15 ± 0.5 GPa, about 1.4 GPa higher than in bulk $^{68}Zn^{76}Se$.

The down-stroke Raman data for the nanorods (Fig. 7b) suggests a reverse transition, but the TO-like peak is weaker after pressure-cycling. (See the pre- and post-transition spectra at similar pressures.) There is also a new peak (arrow) in the 0.2 GPa spectrum, which may have a similar origin to peak 4 in the down-stroke spectra for $^{68}Zn^{76}Se$ (Fig. 5b, lowest trace).

Figure 7c shows a post-transition spectrum at 1.6 GPa and 140 K for a bulk $^{68}Zn^{76}Se$ sample. This sample was maintained below 160 K during the entire experiment, including the forward and reverse transitions. The Fig. 7c spectrum is remarkably similar to the ZnSe nanorod results at 1.9 GPa and 1.5 GPa in Fig. 3b. However, it differs substantially from the spectrum in Fig. 5b at 1.6 GPa for bulk $^{68}Zn^{76}Se$ cycled through its transitions at 300 K. These results indicate that the bulk sample kept at low temperature has fragmented into domains with localization comparable to the ~5 nm × 20 nm nanorods. However, the domains in the bulk sample kept at 300 K re-grow to a much larger size, again suggesting the important role of kinetics, this time in the reverse transition [43].

Notice also that the pre-transition broadening is different in the nanorod and bulk ZnSe spectra. For the nanorods (Fig. 7a) the effect occurs at much lower pressures than the broadening (at similar frequencies) in bulk $^{68}Zn^{76}Se$ (Fig. 5b). We suspect that the nanorods are affected by cluster agglomeration. The

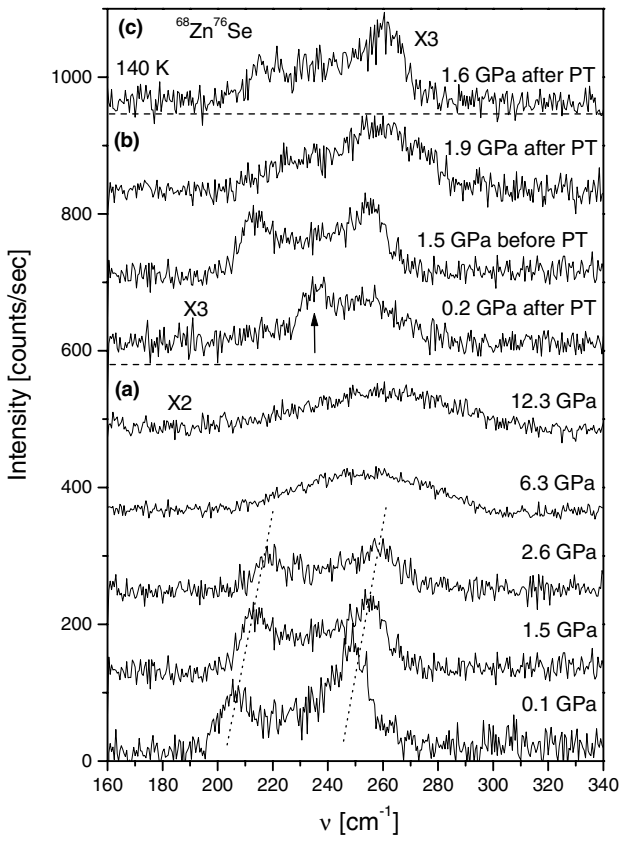

Fig. 7 (a) Up-stroke Raman spectra for ZnSe nanorods at 300 K; (b) pre- and post-transition nanorod spectra; (c) post-transition spectrum of $^{68}Zn^{76}Se$ at 1.6 GPa and 140 K in a He medium.

low-pressure broadening in the nanorod spectra may result from non-homogeneous surface strain at particle contact points, or from the effects of interparticle dipole–dipole coupling on the nanorod modes. More experiments are needed to clarify these issues.

3 Pressure-Raman studies of InP/CdS core/shell nanoparticles

The InP/CdS core/shell nanoparticle system offers interesting possibilities to study the interaction and decay of vibrational modes because the bulk TO(Γ) phonon of InP at 303 cm^{-1} and the bulk LO(Γ) phonon of CdS at 305 cm^{-1} overlap in frequency [44, 45].

We review briefly the properties of normal modes in spherical nanoparticles which have been calculated in some detail for both homogeneous and core/shell systems. (See for example Refs. [2, 3].) In curvilinear coordinates, the displacements take the form

$$\begin{aligned} &\boldsymbol{u} = u_{\mathrm{T}}\hat{e}_r + u_{\mathrm{T}}\hat{X}_{\mathrm{lm}} + u_{\mathrm{LT}}\hat{e}_r \times \hat{X}_{\mathrm{lm}}, \quad \text{with} \quad \hat{e}_r = \frac{\hat{r}}{r}, \\ &\hat{X}_{\mathrm{lm}} = [l(l+1)]^{-1/2}\boldsymbol{L}Y_{\mathrm{lm}}(\theta,\varphi), \quad \text{and} \quad \boldsymbol{L} = -i\hat{e}_r \times \nabla . \end{aligned} \tag{2}$$

Simple boundary conditions are chosen such that the electric potential Φ and $\varepsilon_\infty \partial\Phi/\partial r$ are continuous, and $\boldsymbol{u} = 0$, at the interfaces. The dielectric continuum model (DCM) embodied in $\varepsilon(\omega)\nabla^2\Phi = 0$ is often applied, leading to confined mode, $\varepsilon(\omega) = 0$, and surface mode, $\nabla^2\Phi = 0$, solutions. However, for small

particles the mechanical boundary conditions and the phonon dispersion modify the DCM results. The general solutions decompose into purely transverse torsional modes $\propto X_{lm}$, and spheroidal modes that can have mixed longitudinal-transverse character. The latter modes with $l = 0$ are purely radial and LO-like, while those with $l \geq 1$ have mixed LO–TO character. The torsional modes should be optically silent for all values of l due to their parity. The spheroidal modes with $l = 0, 2$ are Raman active; those with $l = 1$ are IR active.

Interactions between the vibrational modes of nanoparticles can arise in many ways. The general loss of $\boldsymbol{q}$-conservation will tend to eliminate gaps in the bulk multiphonon DOS (such as affect the TO and LO peaks in $^{68}Zn^{76}Se$), and this, combined with the mixed LO–TO character of modes, should increase the channels for anharmonic decay. Deviations from spherical shape can produce further mixing. In addition, for the InP/CdS core/shell system, the frequency overlap of the InP TO(Γ) and CdS LO(Γ) bulk phonons relaxes the $\boldsymbol{u} = 0$ boundary constraint, raising the possibility of cross-interface mechanical coupling of modes in the core and shell regions.

InP/CdS nanoparticles were grown in a two-stage colloidal process using trimethylsilyl myristate as the surfactant [46]. From TEM, X-ray and EDS characterization, the sample ensemble contained particles ~5–11 nm in total diameter with shell-to-core diameter ratios ~1.2–1.7. The nanoparticles appear to have mixed zincblende-wurtzite structure. Raman spectra were recorded as a function of decreasing temperatures at 1 atm (Fig. 8), and as a function of applied pressure at 300 K (Fig. 9). For the former experiments, the nanoparticles were dispersed in a CsI matrix, and for the latter they were loaded as a powder in the DAC with 4 : 1 methanol : ethanol medium.

The spectra in Fig. 8 show three features. The arrows mark assignments made using DCM calculations [47]. The InP LO-like $l = 0$ peak is clearly seen. The peak at 300–325 cm^{-1} falls just above the bulk InP TO(Γ) and CdS LO(Γ) frequencies. In principle it is a mixture of the $l = 2$ mode of the core and a SO mode at the core-shell interface. The low energy shoulder is in the region of other shell-related SO modes [48]. Similar shoulders appear in the Raman spectra of other nanoparticles and are often described by a sum of SO and confined modes without considering coupling between these modes [3, 5].

In Fig. 9 we observe that the InP TO-like and LO-like peaks tend to merge with increasing pressure. The measured pressure-shifts are (6.7 ± 0.7) cm^{-1}/GPa and (5.0 ± 0.5) cm^{-1}/GPa, respectively, very similar to the TO(Γ) and LO(Γ) pressure coefficients of bulk InP [44]. The low-energy band attributed to the CdS shell-modes broadens further under pressure, and only is seen contributing to the tail of the InP TO-

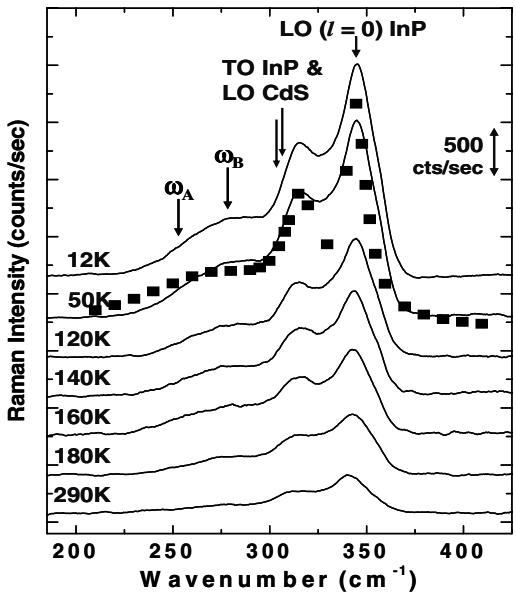

Fig. 8 Observed Raman spectra of InP/CdS nanoparticles vs. temperature at 1 atm from Ref. [47]. ω_A and ω_B are SO modes of the CdS shell. Solid squares are calculated.

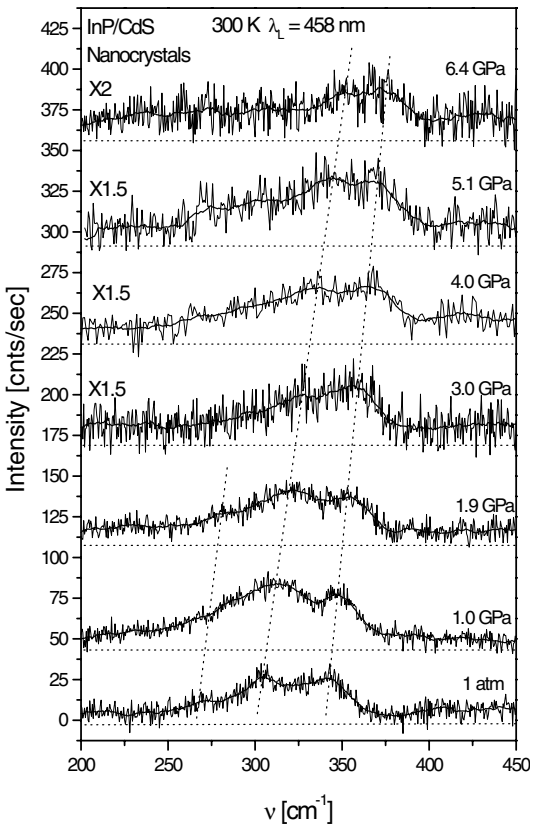

Fig. 9 Pressure-Raman spectra of InP/CdS nanoparticles at 300 K. Dashed lines show approximate shift of three main spectral features. Solid curves computed by numerical smoothing.

like peak. The overall decrease in intensity of the spectra at higher pressures may be related to the onset of a sluggish phase transition in the CdS shells. Rapid visual darkening of the sample was observed at 8.9 GPa. Since the bulk thresholds are P_T(CdS) ~2.7 GPa [45] and P_T(InP) ~ 10.8 GPa [49], and the P_T of nanoparticles are expected to be elevated, we attribute the 8.9 GPa darkening to the final onset of the transition in the CdS shells.

The Raman line-shape in confined systems is sometimes treated *via.* the spatial correlation model [41],

$$I(\omega) \propto \int \frac{\Gamma \exp(-\boldsymbol{q}^2 L^2/4)}{[\omega - \omega_0(\boldsymbol{q})]^2 + [\Gamma/2]^2} \, \mathrm{d}^3\boldsymbol{q} \,, \tag{3}$$

which includes in an average way modes within a span $\Delta\boldsymbol{q} \sim 1/L$, where L is the typical confinement length. This approach has been used successfully to analyze the Raman spectra of porous Si and other disordered nanocrystalline systems [32, 50]. In principal, specific phonon decay paths could be included by introducing (as in Eq. (1)) a dispersive line-width $\Gamma(\omega)$, proportional to the *effective* DOS $\rho_D(\omega)$ into which the modes couple. As remarked, one expects that $\rho_D(\omega)$ will include many more decay paths in nanoparticles than in bulk crystals, and in the InP/CdS core/shell system the overlapping phonon frequencies suggests that cross interface mechanical coupling should be considered.

The Raman line-shape in Fig. 8 was simulated (solid squares) using a sum of three $I(\omega)$-term*s* from Eq. (3), each with different $\omega_0(\boldsymbol{q})$ to represent the LO-like and TO-like modes of the InP core, and the modes of the CdS shell. We chose q^2-dispersions appropriate to the bulk phonon branches of each material, and used $L = 30$ Å (in between the ~50 Å core diameter and ~15 Å shell thickness). A reasonable fit could be found using non-dispersive line-widths: Γ_{LO}(InP) = 13 cm^{-1}, Γ_{TO}(InP) = 20 cm^{-1},

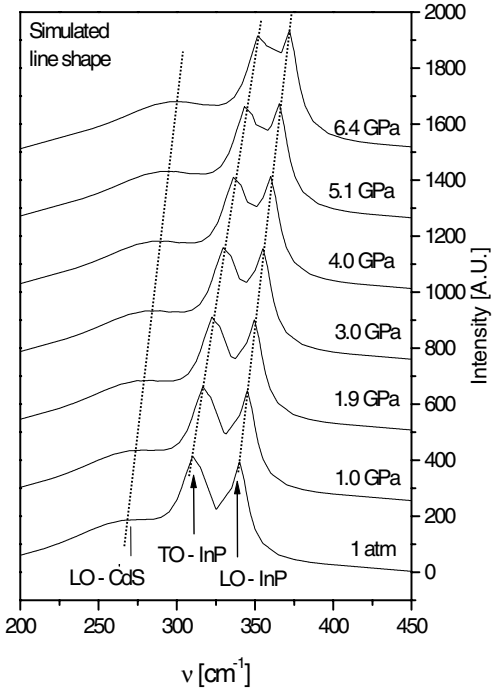

Fig. 10 Simulation of InP/CdS Raman line-shape at different pressures using model in text.

Γ_{LO}(CdS) = 96 cm^{-1}; the large value of the latter reflects the broad span of SO modes and the degree of disorder expected in these thin-shelled nanocrystals.

In Fig. 10, we explore the effect of increasing pressure on this simulated Raman spectrum. The three features in the line-shape were allowed to shift at the rates measured in this work for the InP LO- and TO-like peaks, and at the rate of the bulk CdS LO(Γ) phonon 4.8 cm^{1}/GPa [45] for the broad low-energy band. The other fitting parameters – Γ-values, localization L, and curvature of the phonon dispersions, were not changed. As expected, the simulation shows the merging of the InP LO- and TO-like peaks. However, this simple calculation using non-dispersive Γ-values cannot reproduce the broadening trend of the low-frequency band indicated in the data for $P \geq 2$ GPa. A possible explanation is that the observed behavior arises from a decrease in cross-interface coupling due to reduced frequency overlap between the InP TO-like modes and the manifold of modes in the CdS shell. The pressure-tuning of this overlap is analogous to the tuning of the resonant anharmonic interaction that affects the line-shape of the TO(Γ) phonon in bulk material, as discussed above in relation to Fig. 4. Additional Raman studies as a function of pressure and temperature on the InP/CdS nanoparticle system will be used to further test this explanation, and to determine the strength of the cross-interface mode coupling.

4 Summary

High-pressure Raman experiments and associated studies of semiconductor nanoparticles have advanced our understanding of the ways in which the stability, localization, and vibrational properties of these systems differ from bulk crystals. Important recent work is reviewed, focusing on phase transition effects. Bulk crystals cycled through their high-pressure transitions often fragment into domains with localization properties that suggest a disordered nanoparticle system. The Raman spectrum of bulk crystalline $^{68}Zn^{76}Se$ is found to exhibit strong broadening in the TO(Γ)–LO(Γ) region for $P \geq 11$ GPa at 300 K. This effect is not seen in $^{68}Zn^{76}Se$ at 11 K, and is too large to be due to multiphonon decay. We suggest that it arises from disorder and nano-scale localization caused by the early nucleation stages of the 4-fold to 6-fold transition in bulk ZnSe. Pressure-Raman results on ZnSe nanorods are presented. Similarities

between the pressure-cycled spectra of bulk $^{68}Zn^{76}Se$ (maintained at $T < 160$ K) and the analogous spectra of nanorod ZnSe support the above explanation for the strong broadening, and indicate the importance of kinetics for the reverse transition path in ZnSe. The effects of pressure on the Raman spectrum of InP/CdS core/shell nanoparticles are investigated. The observed broadening of the CdS shell-mode band under pressure may be related to variations in cross-interface mechanical coupling.

Acknowledgements The author gratefully acknowledges the assistance of R. E. Tallman, H. Zeng, and W. Shi at the University of Buffalo, and R. Lauck and M. Cardona at the Max-Planck Institut, Stuttgart, for their valuable assistance and consultation on many aspects of the present work.

References

[1] A. D. Yoffe, Adv. Phys. **50**, 1 (2001).
[2] E. Roca, C. Trallero-Giner, and M. Cardona, Phys. Rev. B **49**, 13704 (1994).
[3] M. P. Chamberlain, C. Trallero-Giner, and M. Cardona, Phys. Rev. B **51**, 1680 (1995).
[4] O. Verzelen, R. Ferreira, and G. Bastard, Phys. Rev. Lett. **88**, 146803 (2002).
[5] T. D. Krauss, F. W. Wise, and D. B. Tanner, Phys. Rev. Lett. **76**, 1376 (1996).
[6] X. Q. Li, H. Nakayama, and Y. Arakawa, Phys. Rev. B **59**, 5069 (1999).
[7] M. Bayer, P. Hawrylak, K. Hinzer, S. Fafard, Z. Wasilewski, O. Stem, and A. Forchel, Science **291**, 451 (2001).
[8] A. Kailer, K. G. Nickel, and Y. G. Gogotsi, J. Raman Spectrosc. **30**, 939 (1999).
[9] K. Jacobs, D. Zaziski, E. Scher, A. Herhold, and A. P. Alivisatos, Science **293**, 1803 (2001).
[10] C. Burda, X. Chen, R. Narayanan, and M. A. El-Sayed, Chem. Rev. **105**, 1025 (2005).
[11] M. Bruchez, M. Morone, P. Gin, S. Weiss, and A. P. Alivisatos, Science **281**, 2013 (1998).
[12] S. H. Tolbert and A. P. Alivisatos, Ann. Rev. Phys. Chem. **46**, 595 (1995).
[13] K. Teo, L. Qin, I. Noordin, Z. Shen, O. Schmidt, K. Eberl, and H. Queisser, Phys. Rev. B **63**, 121306 (2001).
[14] C. J. Lee, A. Mizel, U. Banin, M. L. Cohen, and A. P. Alivisatos, J. Chem. Phys. **113**, 2016 (2000).
[15] J. Hung, S.-C. Lee, and C.-Ta. Chia, J. Nanoparticle Res. **6**, 415 (2004).
[16] J. Schroeder and P. D. Persans, J. Lumin. **70**, 69 (1996).
[17] K. Jacobs, J. Wickham, and A. P. Alivisatos, J. Phys. Chem. **106**, 3759 (2002).
[18] G. Hearne et al., Phys. Rev. B **70**, 134102 (2004).
[19] S. Chen, Y. C. Liu, C. Shao, C. Xu, Y. X. Liu, L. Wang, B. Liu, and G. Zou, J. Appl. Phys. **98**, 106106 (2005).
[20] A. P. Alivisatos, J. Phys. Chem. **100**, 13226 (1996).
[21] P. Freie, M. Araujo-Silva, V. Reynoso, and V. Lemos, Phys. Rev. B **55**, 6743 (1997).
[22] K. Joseph Wilson and K. Navaneethakrishnan, phys. stat. sol. (b) **242**, 2515 (2005).
[23] J. Zeman, M. Zigone, G. Rikken, and G. Martinez, J. Phys. Chem. Solids **56**, 655 (1995).
[24] C. Campos, J. Lima, T. Grandi, J. Itie, A. Polian, and A. Michalowicz, J. Phys.: Condens. Matter **17**, 5187 (2005).
[25] J. Gonzalez et al., High Press. Res. **25**, 119 (2005).
[26] A. P. Alivisatos, T. D. Harris, L. E. Brus, and A. Jayaraman, J. Chem. Phys. **89**, 5979 (1988).
[27] M. Hasse and A. P. Alivisatos, J. Phys. Chem. **96**, 6756 (1992).
[28] S. H. Tolbert and A. P. Alivisatos, Science **265**, 373 (1994).
[29] L. Qin, K. L. Teo, Z. X. Shen, C. S. Peng, and J. M. Zhou, Phys. Rev. B **64**, 075312 (2001).
[30] K. Jacobs, D. Zasiski, E. C. Scher, A. B. Herhold, and A. P. Alivisatos, Science **293**, 1803 (2001).
[31] J. N. Wickham, A. B. Herhold, and A. P. Alivisatos, Phys. Rev. Lett. **84**, 923 (2000).
[32] M. Kobayashi, H. Iwata, T. Horiguchi, and S. Endo, phys. stat. sol. (b) **198**, 521 (1996).
[33] J. Serrano, A. Cantarero, M. Cardona, N. Garro, R. Lauck, R. E. Tallman, T. M. Ritter, and B. A. Weinstein, Phys. Rev. B **69**, 014301 (2004).
R. E. Tallman et al., phys. stat. sol. (b) **241**, 3143 (2004).
[34] A. Debernardi, C. Ulrich, M. Cardona, and K. Syassen, phys. stat. sol. (b) **223**, 213 (2001).
[35] C. Ulrich, A. Gobel, K. Syassen, and M. Cardona, Phys. Rev. Lett. **82**, 351 (1999).
[36] D. N. Talwar, M. Vandevyver, and K. Kunc, Phys. Rev. B **24**, 741 (1981).
[37] Similar results were found in isotope-mixed natural ZnSe. See: B. Weinstein, Solid State Commun. **24**, 595 (1977).

[38] J. Pellicer-Porres, A. Segura, V. Munoz, J. Zuniga, J. Itie, A. Polian, and P. Munsch, Phys. Rev. B **65**, 012109 (2001).
[39] A. Qteish and A. Munoz, J. Phys.: Condens. Matter **12**, 1705 (2000).
[40] A. K. Bandyopadhyay and L. C. Ming, Phys. Rev. B **54**, 12049 (1996).
[41] I. H. Campbell and P. M. Fauchet, Solid State Commun. **58**, 739 (1986).
[42] P. Teredesai, L. Deepak, A. Govindaraj, A. K. Sood, and C. N. R. Rao, J. Nanosci. Nanotechnol. **2**, 495 (2002).
[43] The Fig. 7c spectrum did not seem to change rapidly with time after the sample was brought to 300 K (1.6 GPa).
[44] R. Trommer, H. Muller, M. Cardona, and P. Vogl, Phys. Rev. B **21**, 4869 (1980).
[45] U. Venkateswaran, M. Chandrasekhar, and H. Chandrasekhar, Phys. Rev. B **30**, 3316 (1984).
[46] D. Lucey, D. MacRae, M. Furis, Y. Sahoo, A. Cartwright, and P. Prasad, Chem. Mater. **17**, 3754 (2005).
[47] F. Manciu, Ph.D. dissertation 2004, unpublished.
[48] F. Comas and C. Trallero-Giner, Phys. Rev. B **67**, 115301 (2003).
[49] C. S. Menoni and I. L. Spain, Phys. Rev. B **35**, 7520 (1987).
[50] Z. Sui, P. P. Leong, I. P. Herman, G. S. Higashi, and H. Temkin, Appl. Phys. Lett. **60**, 2086 (1992).

